Thermochimica Acta, 88 (1985) 127—142
Elsevier Science Publishers B.V., Amsterdam — Printed in The Netherlands

HIGH-RESOLUTION AC CALORIMETRY AND CRITICAL BEHAVIOR AT PHASE TRANSITIONS

Carl W. Garland
Department of Chemistry and Center for Materials Science and Engineering,
Massachusetts Institute of Technology, Cambridge, Massachusetts 02139 (USA)

ABSTRACT

An AC calorimeter technique operating at very low frequencies has been developed for the study of second-order phase transitions. Only a small amount of sample is required (50 to 100 mg), and samples with low thermal conductivity, such as insulator crystals, fluids and liquid crystals, can be investigated at 1 atm and at pressures up to ~3000 bar. Two versions of this AC calorimeter will be described: a manually operated high-precision (±0.05%) calorimeter with a computerized data-acquisition system, and a fully computerized calorimeter with good precision (±0.2%) which can be operated in a scanning mode with linear drift rates in the range 0.01 K/hour to 1 K/hour. Experimental results and a discussion of their analysis will be presented for order-disorder transitions in ionic crystals (ammonium halides), consolute-point phase separation in binary liquids (3-methylpentane + nitroethane), orientational ordering in aqueous micelle solutions (cesium perfluoro-octanoate), and a variety of liquid crystal systems (with emphasis on transitions involving nematic and various smectic phases).

INTRODUCTION

AC calorimetry is a calorimetric technique in which a small oscillatory heat input is supplied to a sample and the heat capacity is determined from the amplitude of the resulting temperature oscillations. This method, which was developed independently by Kraftmakher (ref.1), Sullivan and Seidel (ref.2) and Handler, Mapother and Rayl (ref.3), has proven very useful for high-resolution studies of second-order phase transitions (refs. 2-4). However, most early investigations were carried out on metal samples, which have high thermal conductivity and permit the use of heating frequencies in the 10-100 Hz range. This paper is concerned with the extension of the AC method to the study of phase transitions in low conductivity solids, fluids and liquid crystals at 1 atm and at high pressures. A summary description of our experimental methods will be given in the next section. The following section will review the results obtained for second-order transitions in ionic crystals, binary liquid mixtures, micellar solutions, and a variety of liquid crystals.

METHODS

In the simplest model for an AC calorimeter, a sample of heat capacity C_p is

0040-6031/85/$03.30

loosely coupled to a heat reservoir (bath) at temperature T_0 by a massless link with thermal conductance Λ. This thermal link is provided in part by the electrical leads and in part by the gas surrounding the sample. Conservation of energy yields

$$P_{in} = \frac{dU}{dt} + P_{out}$$

$$P_0 + P_1 \exp(i\omega t) = C_p \frac{d(\Delta T)}{dt} + \Lambda \Delta T \tag{1}$$

where P_{in} is the input power, an oscillatory input due to AC resistive heating, and $P_{out} = \Lambda \Delta T$ is the rate of heat loss to the bath. The sample temperature T is related to the bath temperature T_0 by $T(t) = T_0 + \Delta T(t)$.

If the period $2\pi/\omega$ is long compared with the time scale for internal heat flow in the sample, the solution to Eq. (1) can be written as

$$\Delta T(t) = \Delta T_{dc} + \Delta T_{ac} \exp(i\omega t + i\phi) \tag{2}$$

where

$$\Delta T_{dc} = P_0/\Lambda \tag{3}$$

$$(P_1/\Delta T_{ac})^2 = \omega^2 C_p^2 + \Lambda^2 \tag{4}$$

$$\tan \phi = -\omega C_p/\Lambda \tag{5}$$

It is convenient to define a quantity $C^* \equiv P_1/\omega \Delta T_{ac}$ in terms of which Eq. (4) can be rewritten as

$$(C^*/C_p)^2 = 1 + (\Lambda/\omega C_p)^2 \tag{6}$$

At atmospheric pressure most experiments are carried out in a frequency regime for which $\omega\tau = \omega C_p/\Lambda \gg 1$, where τ is the thermal relaxation time between the sample and the bath. Thus

$$C_p \cong P_1/\omega \Delta T_{ac} \tag{7}$$

is an excellent approximation at 1 atm. Measurements at high pressure require a more sophisticated analysis, the details of which are given elsewhere (refs. 5 and 6).

The sample cell for fluids or liquid crystals is shown in Fig. 1. The body of the cell is a cup 1 cm in diameter and 0.12 cm deep pressed from 0.01-in. silver sheet. A lid of 0.003-in. silver foil is attached using a cold-welded indium or solder seal. The filled cell weighs ~600 mg and contains 50-100 mg of sample. Three or four short (0.2 cm) nickel rods were used for magnetic stir-

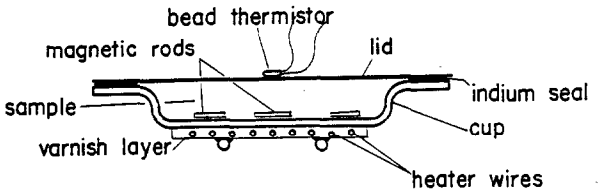

Fig. 1. Sample cell for liquids.

ring in the study of binary mixtures near their consolute point. In the case of liquid crystals, these rods are replaced by a long coil of fine gold wire, which greatly increases the effective internal thermal conductivity. The AC heat input is supplied by a resistance heater, and the resulting temperature oscillations (ΔT_{ac}) are measured with a microbead thermistor. For the study of crystals, the silver sample cell is not used, and the heater and thermistor are cemented directly onto a crystal slab with dimensions of approximately 1 × 1 × 0.05 cm (refs. 7 and 8).

The basic design features for our AC calorimeter are described in ref. 6. In that work and several subsequent studies (refs. 8-14), the thermistor comprised one arm of a sensitive ac resistance bridge driven at 1050 Hz. The temperature oscillations $\pm\Delta T_{ac}$ about the mean sample temperature $T_o + \Delta T_{dc}$ caused a bridge imbalance signal, which was observed as a slow sinusoidal variation in the output of a lock-in amplifier that served as the null detector. This output signal was digitized and stored in the memory of a microcomputer. Successive periods were overlaid in memory until good signal averaging was obtained (usually 20 to 40 periods). The stored data were then Fourier analyzed for the amplitude ΔT_{ac} and the phase ϕ, and a correction was applied to account for bath temperature drifts during the ~20 min of data acquisition. Data obtained in this fashion were well represented by Eq. (4) over the range $0.06 < \omega < 0.3$, where $\omega = 2\pi(2f_H)$ and f_H is the heater frequency.

The technique described above provided high precision ($\pm 0.05\%$ for C_p) but was tedious in operation since it required a manual setting of the bath thermostat and bridge balance every 30 min and manual readings of the input power and platinum thermometer. Fortunately, we have determined recently that the quality of the results is not greatly affected if direct thermistor resistance readings are made with a Keithley model 192 programmable digital multimeter. This has allowed us to develop a convenient and fully computerized version of the ac method (refs. 15 and 16).

A block diagram of the new version is given in Fig. 2. This system operates at a constant frequency $\omega = 0.1963$ (corresponding to an exactly 32-sec period for the temperature oscillations). A multiplexer allows the Keithley to measure

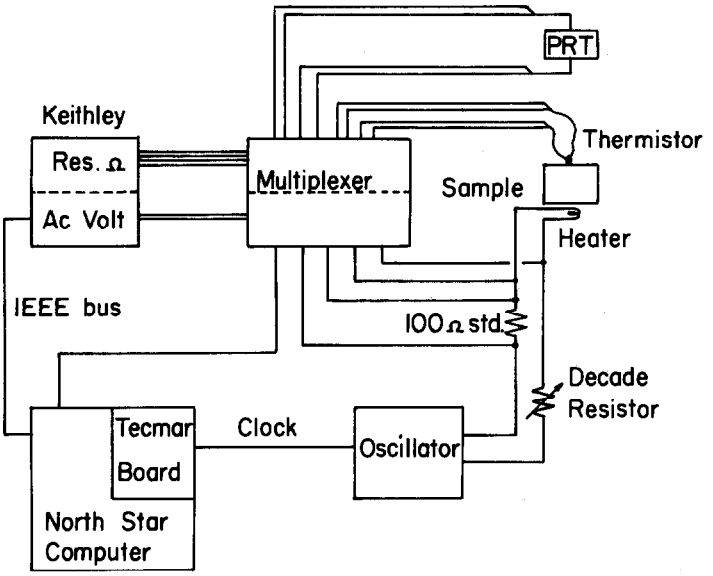

Fig. 2. Block diagram of automated AC calorimeter.

successively the heater current, the heater voltage, the platinum thermometer resistance, and then to measure the thermistor resistance every 0.5 sec during eight periods of oscillation. A typical ΔT_{ac} temperature amplitude of ±5 mK (see Fig. 3) corresponds to a resistance variation of $\Delta R \simeq 50\Omega$ for a thermistor with R = 60 kΩ. The Keithley 192 is capable of 6.5 decades of resolution, and the typical scatter in the C_p values is ±0.2%. The oscillator and the thermistor reading times are synchronized by the computer, which allows a quite simple calculation of ΔT_{ac} and ϕ from Fourier sine and cosine sums over the stored data set of 512 thermistor readings. As before, the data are corrected for any drift in the average temperature of the sample over the duration of a given data point. This is accomplished by fitting a polynomial to thermistor readings that correspond to the "zero crossings" of the heater input and subtracting the resulting curve from the data set. The temperature of the thermostat bath can be held constant during the taking of each data point or can be slowly scanned up or down in temperature. Near second-order transitions, a very slow scan rate (12 mK h^{-1}) was used. There was no indication of hysteresis on warming or cooling, and the data obtained with such scans agreed with data taken at constant bath temperatures. Thus we believe that full thermodynamic equilibrium is achieved during these slow scans.

This new automated version of our AC calorimeter has been used in several recent studies of binary fluid mixtures (ref. 15), liquid crystals (refs. 16-20),

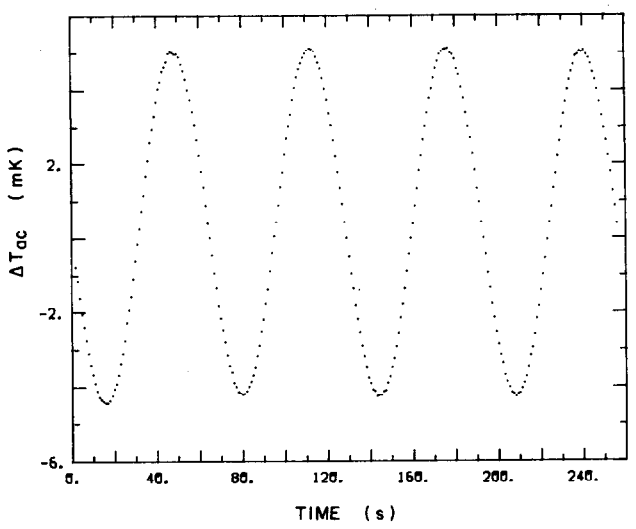

Fig. 3. Typical sample temperature oscillations during data acquisition (only four periods shown).

and micellar solutions (ref. 21). Different versions of AC calorimetry that are also suitable for the study of second-order phase transitions have been developed by others; see, for example, methods developed by Johnson (ref. 22), Huang (ref. 23), and Hatta (ref. 24). Our method has the advantages of (a) compatibility with high-pressure operation, (b) a sealed cell that prevents chemical reaction with the atmosphere, and (c) providing absolute C_p values (although the accuracy of the absolute values is only 5 to 10%).

It should be stressed that AC calorimetry measures the heat capacity C_p directly and does not measure the enthalpy H. Thus, the magnitude of discontinuous enthalpy changes (latent heats ΔH) cannot be determined. However, the occurrence of a first-order transition can be detected qualitatively by an anomously large value of C_p and an associated abrupt shift in the phase ϕ when two coexisting phases are present in the cell. The sensitivity of our AC calorimetry for observing second-order transitions is comparable to that of commercial differential scanning calorimeters, and the absolute accuracy of the integrated enthalpy $\delta H = \int \Delta C_p dT \equiv \int [C_p - C_p(\text{background})] dT$ is much higher. Phase transitions with integrated enthalpies δH greater than 0.03 J/g can be detected, and the critical C_p temperature dependence can be characterized accurately for second-order transitions with $\delta H > 0.1$ J/g.

APPLICATIONS

Let us begin this section with a very brief review of the heat-capacity behavior expected at a second-order phase transition according to the Landau model

and various critical fluctuation models (such as the Ising, XY, and Heisenberg models). For the Landau model, fluctuations do not play a significant role near the transition temperature T_c and the Gibbs free energy can be taken to have the form

$$G = G_0 + at\psi^2 + b\psi^4 + c\psi^6 \tag{8}$$

where ψ is the order parameter and the reduced temperature t is defined by $t \equiv (T - T_c)/T_c$. Equation (8) leads to

$$C_p = \begin{cases} C_p^0 & \text{for } T > T_c \\ C_p^0 + A\frac{T}{T_c}\left(\frac{T_k - T_c}{T_k - T}\right)^{1/2} & \text{for } T < T_c \end{cases} \tag{9}$$

where $A \equiv a^2/2bT_c$, and $T_k = T_c + b^2T_c/3ac$ represents the metastability limit (ref. 25). The quantity C_p^0, the background heat capacity arising from the term G_0, usually has the form $B + E(T - T_c)$. The Landau coefficients a and c are always positive, but b can have either sign. If $b < 0$, the transition will be first order. If $b > 0$, a second-order transition occurs at T_c and the heat capacity undergoes a discontinuous jump of magnitude A at T_c. The temperature dependence of C_p below T_c depends on the relative magnitudes of the Landau coefficients a, b and c. For the limiting case $b = 0$, one obtains a classical tricritical point where C_p goes to infinity like $t^{-0.5}$. Note that in the Landau model, the excess heat capacity due to the occurrence of the phase transition always drops discontinuously to zero as soon as T exceeds T_c.

Models that include the effects of critical fluctuations near T_c lead to the following form for the heat capacity

$$C_p = \begin{cases} At^{-\alpha}(1 + Dt^{0.5}) + B + E(T - T_c) & \text{for } T > T_c \\ A'|t|^{-\alpha}(1 + D'|t|^{0.5}) + B + E'(T - T_c) & \text{for } T < T_c \end{cases} \tag{10}$$

where we have used the scaling equalities $\alpha = \alpha'$ and $B = B'$ and have approximated the corrections-to-scaling exponent Δ_1 by 0.5. One would also expect $E = E'$ since the linear term arises from regular (noncritical) contributions to the free energy. Renormalization group theory supports this form for the critical heat capacity and provides theoretical values for the critical exponents of various universality classes (refs. 26-27). For example, the Ising model (involving a one-component vector order parameter) yields $\alpha_I = 0.110$, whereas the XY model (a two-component vector order parameter) yields $\alpha_{XY} = -0.026$. A negative exponent α means that the critical heat capacity exhibits a finite cusp at T_c

rather than the infinite singularity associated with a positive α value. Note that the power-law singularity given by Eq. (10) predicts a critical heat capacity both above and below T_c, with a predictable amplitude ratio A/A' for any given universality class.

If the phase transition is first order, the Landau expression, Eq. (9), is still valid but the transition occurs at a temperature T_1, where $T_k > T_1 > T_c$ (ref. 8). For very weakly first-order transitions in which fluctuations are important, it is common practice to use Eq. (10) with different effective critical temperatures for fitting data above $T_1(T_c^+ < T_1)$ and below $T_1(T_c^- > T_1)$.

Typical examples of experimental results obtained with our AC calorimeter are presented below for (1) order-disorder transitions in ionic crystals (ammonium halides), (2) critical phase separation in a binary liquid mixture (3-methylpentane + nitroethane), (3) orientational ordering in an aqueous micelle solution (cesium perfluoro-octanoate), and (4) a variety of transitions in smectic liquid crystals.

Ionic crystals

As examples of order-disorder transitions in ionic crystals, results will be shown for the critical heat capacity associated with orientational phase transitions in NH_4Cl, NH_4Br, and $NH_4Br_xCl_{1-x}$ mixed crystals (ref. 8). Order-disorder phenomena in ammonium halide crystals involve a competition between direct octopole-octopole interactions among the NH_4^+ ions and indirect interactions arising from coupling between NH_4^+ orientations and transverse phonons. At room temperature, the NH_4^+ ions are distributed at random with respect to two equivalent right/left orientations. (Disordered ammonium salts have a CsCl-type structure with each NH_4^+ ion surrounded by eight halide ions.) The direct interaction, which favors parallel NH_4^+ orientations, leads to a cubic ordered phase with all NH_4^+ ions oriented in the same way ("ferro-ordered"). This type of ordering is observed in NH_4Cl. The indirect interactions stabilize a tetragonal "antiferro-ordered" phase in which antiparallel chains of NH_4^+ ions run along the tetragonal axis (i.e., a chain of right-oriented NH_4^+ ions is surrounded by four chains of left-oriented ions and vice versa). This type of ordering occurs in NH_4Br and in mixed crystals with $x > 0.08$. See refs. 7, 8 and 28 for further details.

The excess heat capacity ΔC_p associated with orientational ordering is shown in Fig. 4 for ferro-ordering and in Fig. 5 for antiferro-ordering. In each case, T_m denotes the temperature at which C_p achieves its maximum value. In obtaining the excess $\Delta C_p = C_p(\text{obs}) - C_p(\text{background})$, we have determined $C_p(\text{background})$ from a smooth interpolation of C_p values over a wide range below and above the transition and $C_p(\text{background})$ is typically ~70 J K^{-1} mol^{-1}.

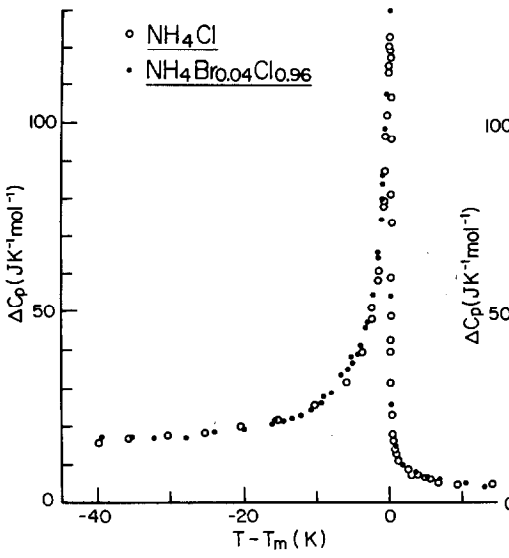

Fig. 4. Excess heat capacity associated with ferro-ordering (ref. 8).

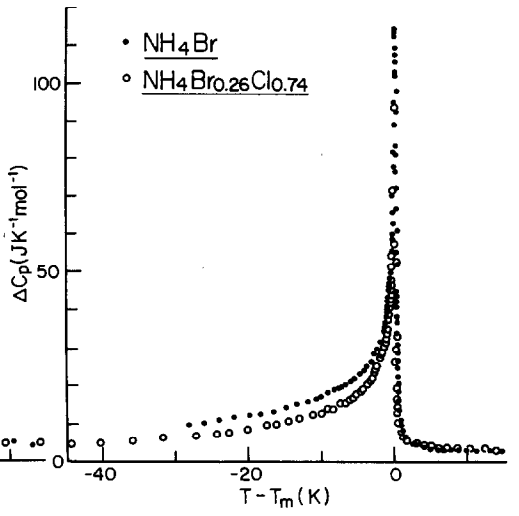

Fig. 5. Excess heat capacity associated with antiferro-ordering (ref. 8).

Analysis of these results is complicated by the fact that all four samples undergo very weak first-order transitions and display coexistence regions of ~80 mK (as indicated by abrupt shifts in the phase ϕ and large jumps in the apparent C_p values). Only data clearly pertaining to a one-phase region are retained in Figs. 4 and 5. The analysis is discussed in detail elsewhere (ref. 8). Suffice it to say here that ferro-ordering is consistent with quasi-tricritical behavior ($\alpha = 0.5$, but $T_c^- > T_1$ as expected for a weak first-order transition near a tricritical point) whereas antiferro-ordering requires an empirical exponent $\alpha = 0.2$. The latter value is difficult to understand within the context of current theoretical models. The best prospect seems to be a crossover from Gaussian behavior far from T_c to cubic ($n = 3$) critical behavior close to T_c. There may also be complications due to inhomogeneous strains in such crystals.

Binary liquid mixtures

Many binary mixtures of two liquid components A and B form homogeneous solutions at high temperatures but separate into coexisting A-rich and B-rich phases on cooling. At the critical composition, such a two-component system exhibits a critical (consolute) point which belongs to the same universality class as the liquid-vapor critical point in a pure fluid and the three-dimensional Ising

model (ref. 29). Thus, C_{px}, the heat capacity at constant pressure and concentration x_c, should diverge with a critical exponent $\alpha = \alpha_I = 0.110 \pm 0.008$.

The observed values of the molar heat capacity $\tilde{C}_{px}$ for the system 3-methylpentane + nitroethane are shown in Fig. 6. This sample had a mole fraction of

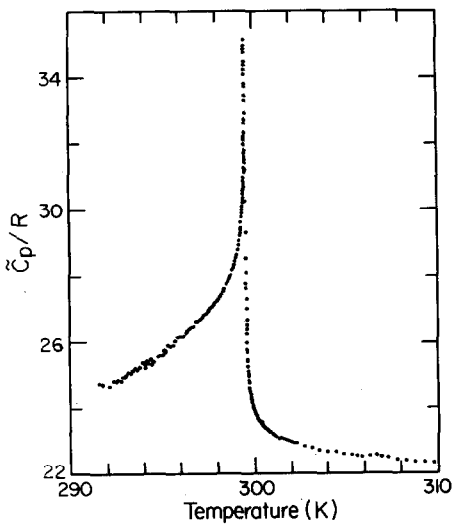

Fig. 6. Heat capacity of a 3-methylpentane + nitroethane critical mixture (ref. 15).

nitroethane x = 0.502 ± 0.001 and a critical temperature T_c = 299.621K, in good agreement with values obtained from other experiments. The best least-squares fit of these data with Eq. (10) yielded $\alpha = 0.119 \pm 0.010$, A = 2.93R, A' = 5.23R, B = 17.27R, D = 0.388, D' = 0.583, where R is the gas constant (ref. 15). This shows that the critical exponent α agrees with the expected Ising value within the limits of error. It is also possible to compare the critical amplitude ratio A'/A with the 3D Ising model value since this ratio is a universal quantity. Our experimental ratio A'/A = 1.79 ± 0.06 agrees within the error bounds with the theoretical ratio 1.95 ± 0.13. Thus, the shape of the critical heat capacity curve (determined by the exponent α and the amplitude ratio A'/A) confirms the prediction that the critical behavior of this binary liquid system belongs to the 3D Ising universality class.

Micellar solutions

When amphiphilic solute molecules are dissolved in water, they will form micelles with the hydrophilic head groups disposed on the surface and the hydrophobic tails contained in the interior. For solutions of nonspherical micelles

at moderate concentrations, the micelles can interact with each other strongly enough to generate long-range orientational ordering. The behavior of the resulting lyotropic nematic liquid crystals is similar to that observed in the thermotropic liquid crystals to be discussed in the last subsection. However, the microscopic scales are quite different since each of the interacting micelles contain hundreds of amphiphilic molecules while the interactions in thermotropic systems are between individual molecules.

An aqueous solution of cesium perfluoro-octanoate (CsPFO), $C_8F_{17}COOCs$, is an attractive system in which to study the lyotropic nematic(N) to isotropic(I) phase transition. CsPFO forms disk-like micelles whose size and shape do not vary appreciably with temperature, and liquid crystal mesophases are observed over a considerable concentration range without the addition of any third component as a co-surfactant (ref. 30). Optical and magnetic birefringence studies in the nematic and isotropic phases have shown that this N-I transition is first order as expected by symmetry but very weakly so (ref. 31).

An AC calorimetric study was carried out on a binary CsPFO + water solution for which the CsPFO mole fraction x = 0.024, which corresponds to 42.5% CsPFO by weight or a molality m = 1.35. The heat capacity of this solution near the N-I transition is shown in Fig. 7, where the data were obtained on a slow

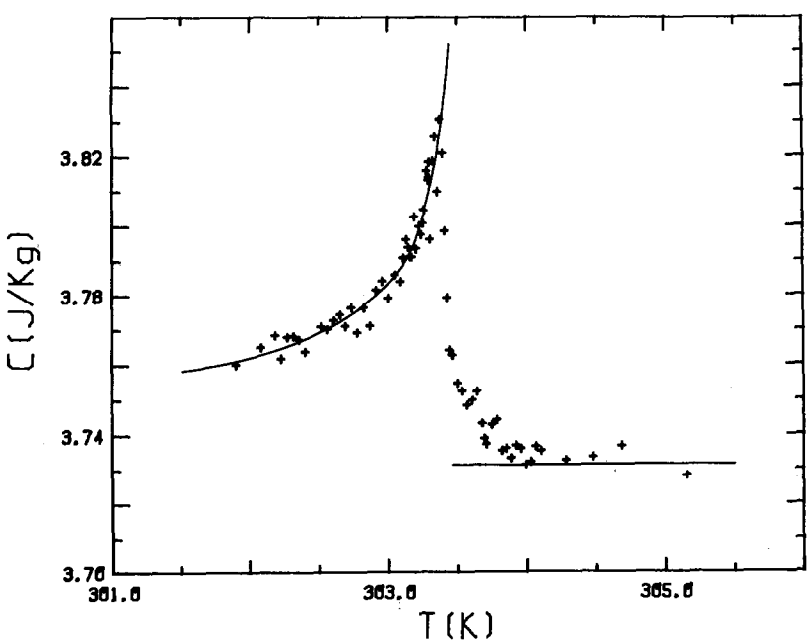

Fig. 7. Specific heat of an aqueous CsPFO micellar solution near the nematic-isotropic transition (ref. 21).

cooling of the sample (ref. 21). Also shown in Fig. 7 is a fit to these data using Eq. (9) with C_p^o = 3.73 J $K^{-1}g^{-1}$, A = 0.125 J $K^{-1}g^{-1}$, T_c = 303.443K, and T_k = 303.539K. In fact, Eq. (9) is not quite correct for this system since the first-order character of the transition arises from the presence of a term in ϕ^3 in the free energy expression [which is not included in Eq. (8)] rather than a negative coefficient b for the ϕ^4 term. However, a more general Landau (mean-field) fit has the same features as that shown in Fig. 7. In particular, C_p drops discontinuously to the background heat capacity above the transition temperature in all mean-field fits. The experimental data show weak pretransitional fluctuation effects above the transition, in qualitative agreement with the N-I behavior in thermotropic liquid crystals (see Fig. 8).

Note that the excess heat capacity due to this lyotropic N-I transition is very small (the peak C_p value is only ~3% greater than the background value).

Liquid crystals

We shall consider here thermotropic liquid crystals that exhibit smectic phases (ref. 32). The systems of interest involve long rod-like organic molecules with an aromatic core and at least one alkyl or alkoxy chain. At sufficiently high temperatures, there is a completely disordered isotropic(I) liquid phase. On cooling, the system transforms into an orientationally ordered nematic(N) phase in which the molecular centers of mass are still translation-

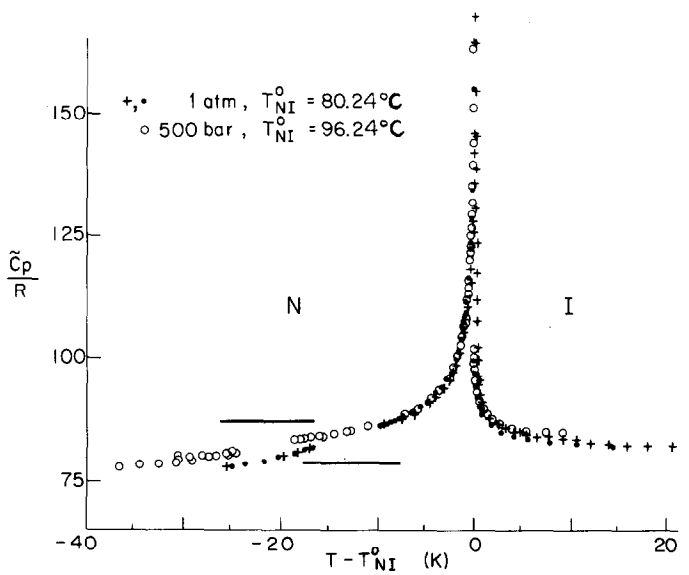

Fig. 8. Heat capacity near the N-I transition in 8OCB (ref. 6). Data points close to the N-SmA transition have been omitted here and are shown in Fig. 9.

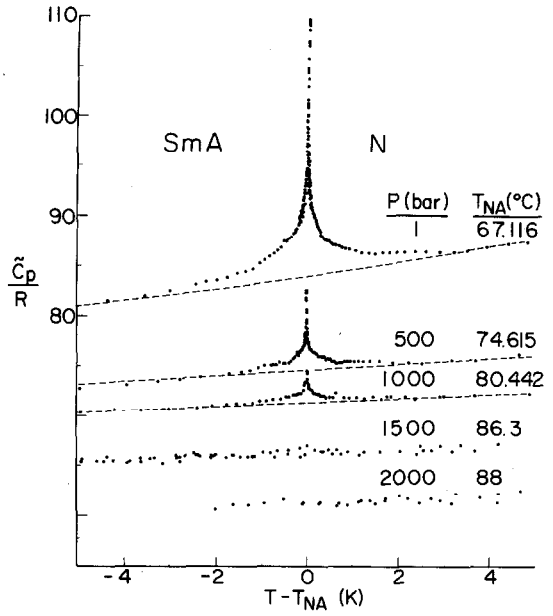

Fig. 9. Effect of pressure on the heat capacity of 8OCB near the N-SmA transition. Each high-pressure curve has been shifted down 5 units (ref. 6).

ally disordered. Further cooling can lead to a layered smectic phase in which there is a one-dimensional density wave (i.e., the z coordinates of the centers of mass are ordered but the system is still translationally liquid-like with respect to the x and y coordinates). There are several types of smectic phase, but we will consider only the smectic-A (SmA) and smectic-C (SmC). In the SmA phase, the local orientational axis (called the director n) is parallel to the direction of the mass-density wave (the z axis). In the SmC phase, n is tilted at an angle with respect to z. A typical example of a nonpolar liquid crystal is butyloxybenzylidene heptylaniline (40.7), for which the SmA layer thickness d equals the molecular length L. In the case of polar liquid crystals such as octyloxycyanobiphenyl (8OCB), a bilayer SmA phase occurs with $d \simeq 1.3L$.

The liquid crystal transitions to be described here are the N-I, N-SmA, and SmA-SmC transitions. The N-I transition is expected theoretically (ref. 32) to be weakly first order, but it has been suggested (ref. 33) that effective tricritical exponents might be observed. The N-SmA and SmA-SmC transitions described here are all second-order.

The heat capacity of 8OCB near the N-I transition is shown in Fig. 8 for pressures of 1 atm and 500 bar. It is clear that there are appreciable pretransitional thermal fluctuations in both the nematic and isotropic phases. Note also that pressure shifts the first-order transition temperature T_{NI}^{o} significantly

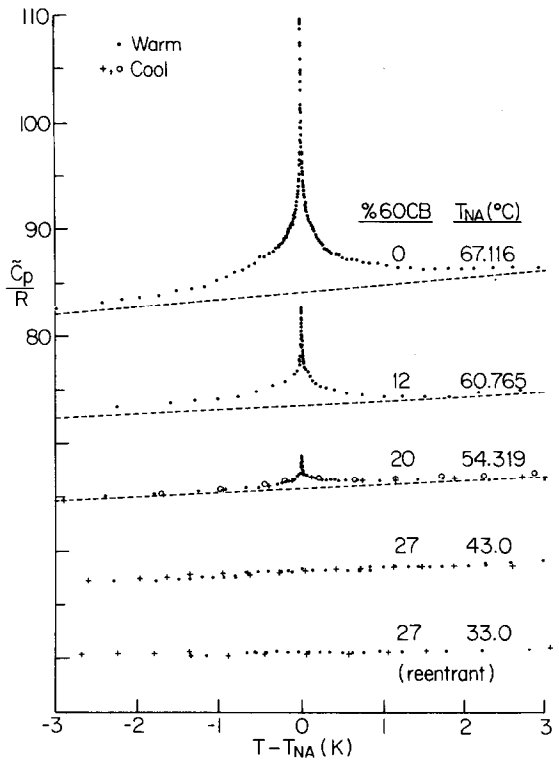

Fig. 10. Effect of composition on the heat capacity of 8OCB + 6OCB mixtures near the N-SmA transition (ref. 11).

but does not affect the size or shape of the heat capacity peak. Fits with Eq. (10) are generally inconsistent with quasi-tricritical behavior but do not firmly establish it; see ref. 6 for further details.

The N-SmA transition in 8OCB gives rise to a sharp and symmetrical heat capacity peak, the magnitude of which is sensitive to the extent of the temperature range of the nematic phase (T_{NI} - T_{NA}). The nematic range can be increased by applying a hydrostatic pressure to pure 8OCB or by making a binary mixture of 8OCB and its shorter chain homolog 6OCB (refs. 6 and 11). The resulting critical heat capacity curves are shown in Figs. 9 and 10. The integrated enthalpy δH_{NA} is 0.33J/g for pure 8OCB and 0.046 J/g for the mixture with 20 wt.% 6OCB. The analysis of the 8OCB data with Eq. (10) yields a critical exponent $\alpha = 0.2 \pm 0.05$ (refs. 6 and 14), which is in serious disagreement with the expected 3D XY behavior (ref. 34) for which $\alpha_{XY} = -0.026$.

Subsequent studies of other smectic compounds show that the effective α value depends strongly on the width of the nematic range. The exponent α approaches the tricritical value of 0.5 in 9CB, which has a narrow nematic range of ~1K

(ref. 35) and the XY value in 40.7, which has a wide nematic range of 26K (ref. 18). The latter result is shown in Fig. 11. Thus, the N-SmA transition (which can be viewed as the simplest kind of freezing transition) is still a considerable challenge to our understanding since no current theory seems capable of explaining all of the available experimental data.

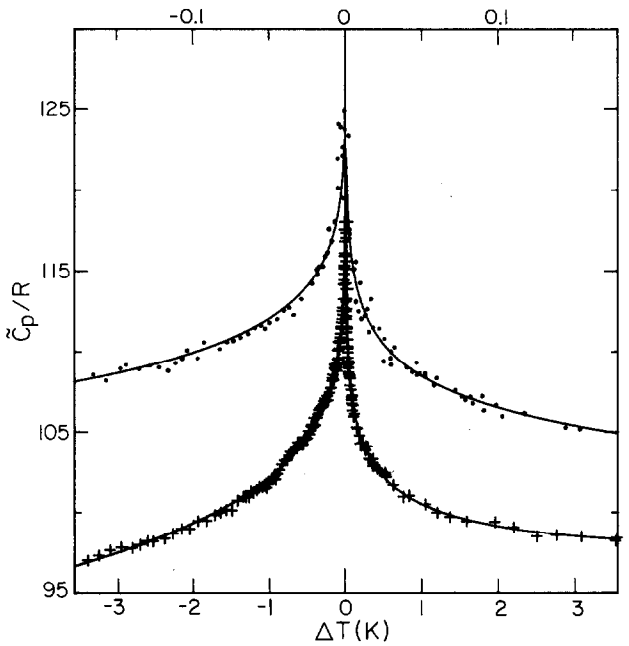

Fig. 11. Detail of the C_p variation near the N-SmA transition in 40.7, for which T_c = 329.75K. The greatly expanded scale at the top is used to show clearly the fit to the data points (•) in the narrow range $|t| < 5 \times 10^{-4}$. The lines show the best fit with Eq. (10) using XY model parameters (ref. 18).

As a final example of AC calorimetric studies of liquid crystals, we present two results for the SmA-SmC transition. Figures 12(a) and 12(b) show that the heat capacity variations near this transition in 40.7 and 70.4 are very well described by mean-field Landau theory. The theoretical model of deGennes predicts that the second-order SmA-SmC transition should be in the same universality class as the 3D XY model. Thus, C_p curves like those in Fig. 12 were expected to have a shape resembling the quite symmetrical curve shown in Fig. 11. However, the mean-field character of SmA-SmC transitions can be understood in terms of the Ginzburg criterion (refs. 16 and 17).

Recently there has been considerable interest in more complex smectic liquid crystals, especially those involving competing interactions that can give rise

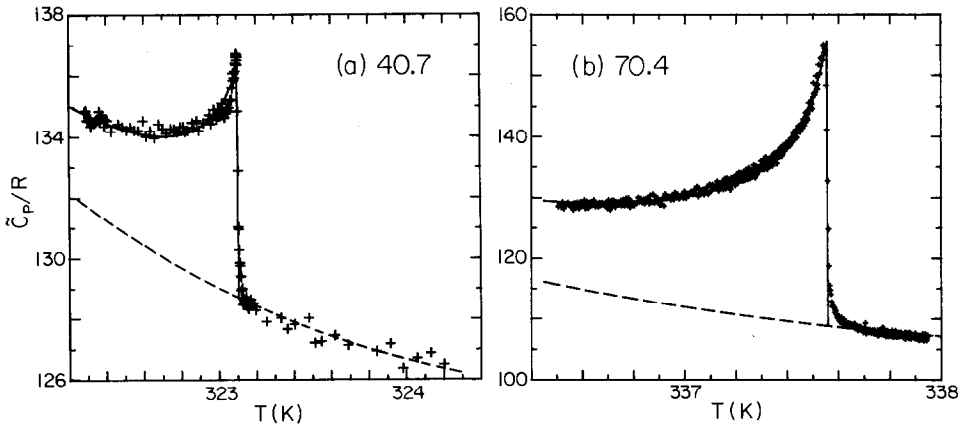

Fig. 12. Heat capacity near the SmA-SmC transition in 40.7(a) and 70.4(b). The solid lines are Landau fits, Eq. (9), using backgrounds (dashed curves) based on the behavior of 40.8 which does not exhibit a SmC phase (see ref. 16 for details).

to several different types of SmA phase in a single material. Various polar liquid crystals with long aromatic cores containing three phenyl rings can exhibit SmA_1 and SmA_2 phases as well as the type of SmA bilayer phase with $d \simeq 1.5L$ observed in shorter molecules such as 8OCB. The SmA_1 phase is a single-layer smectic (with layer thickness d equal to the molecular length L) which shows fluctuations associated with cybotactic bilayer regions. The SmA_2 phase corresponds to a highly ordered smectic phase with two distinct but commensurate layer spacings $d_1 = L$ and $d_2 = 2L$. AC calorimeter studies are providing vital information for characterizing the nature of the critical fluctuations at the new phase transitions seen in such systems (refs. 19-20). Of particular interest is the SmA_1-SmA_2 transition that occurs in mixtures of cyanobenzoyloxybenzoate of hexylphenyl (DB_6) and terephtal-bis-butyl aniline (TBBA). Although it was theoretically predicted that the SmA_1-SmA_2 transition should belong to the Ising universality class with a critical heat capacity exponent $\alpha_I = 0.11$, our experimental study showed that $\alpha = -0.15$ (ref. 20). This negative exponent corresponds to a finite cusp in C_p rather than the expected divergence to infinity.

The work presented in this paper was supported by the National Science Foundation under grants DMR-81-19295 and DMR-83-15637.

REFERENCES

1 Y. A. Kraftmakher, Zh. Prikl. Mekhan. i Tekhn. Fiz., 5 (1962) 176.
2 P. Sullivan and G. Seidel, Phys. Rev., 173 (1968) 679.
3 P. Handler, D. E. Mapother and M. Rayl, Phys. Rev. Lett., 19 (1967) 356.

4 M. B. Salomon, D. S. Simons and P. R. Garnier, Solid State Comm., 7 (1969) 1035.
5 J. D. Baloga and C. W. Garland, Rev. Sci. Instrum., 48 (1977) 105
6 G. B. Kasting, K. J. Lushington and C. W. Garland, Phys. Rev., B22 (1980) 321.
7 C. W. Garland and J. D. Baloga, Phys. Rev., B16 (1977) 331.
8 K. J. Lushington and C. W. Garland, J. Chem. Phys., 72 (1980) 5752.
9 C. W. Garland, G. B. Kasting and K. J. Lushington, Phys. Rev. Lett., 43 (1979) 1420.
10 G. B. Kasting, C. W. Garland and K. J. Lushington, J. Phys. (Paris), 41 (1980) 879.
11 K. J. Lushington, G. B. Kasting and C. W. Garland, Phys. Rev., B22 (1980) 2569.
12 K. J. Lushington, G. B. Kasting and C. W. Garland, J. Phys. Lett. (Paris), 41 (1980) L-419.
13 E. Bloemen and C. W. Garland, J. Phys. (Paris), 42 (1981) 1299.
14 R. J. Birgeneau, C. W. Garland, G. B. Kasting and B. M. Ocko, Phys. Rev., A24 (1981) 2624.
15 G. Sanchez, M. Meichle and C. W. Garland, Phys. Rev., A28 (1983) 1647.
16 M. Meichle and C. W. Garland, Phys. Rev., A27 (1983) 2624.
17 R. J. Birgeneau, C. W. Garland, A. R. Kortan, J. D. Litster, M. Meichle, B. M. Ocko, C. Rosenblatt, L. J. Yu and J. Goodby, Phys. Rev., A27, (1983) 1251.
18 C. W. Garland, M. Meichle, B. M. Ocko, A. R. Kortan, C. R. Safinya, J. J. Yu, J. D. Litster and R. J. Birgeneau, Phys. Rev., A27 (1983) 3234.
19 C. Chiang and C. W. Garland, Mol. Cryst. Liq. Cryst., in press.
20 C. W. Garland, C. Chiang, and F. Hardouin, Phys. Rev., to be published.
21 C. Chiang, C. W. Garland, S. Kumar, B. D. Larson, J. D. Litster and C. Rosenblatt, Tenth International Liquid Crystal Conference, York (1984); to be published.
22 C. A. Schantz and D. L. Johnson, Phys. Rev., A17 (1978) 1504.
23 C. C. Huang, J. M. Viner, R. Pindak and J. W. Goodby, Phys. Rev. Lett., 46 (1981) 1289; C. C. Huang, private communication.
24 S. Imaizumi, K. Suzuki and I. Hatta, Rev. Sci. Instrum., 54 (1983) 1180.
25 L. D. Landau and E. M. Lifshitz, Statistical Physics, Addison-Wesley, Reading, Mass., 1958, sec. 138.
26 J. C. LeGuillon and J. Zinn-Justin, Phys. Rev. Lett., 39 (1977) 95.
27 S.-K. Ma, Modern Theory of Critical Phenomena, Benjamin, Reading, Mass., 1976.
28 C. W. Garland, K. J. Lushington and R. C. Leung, J. Chem. Phys., 71 (1979) 3165.
29 J. V. Sengers and J. M. H. Levelt-Sengers, in C. A. Croxton (Ed.), Progress in Liquid Physics, Wiley, New York, 1978, p. 103 ff.
30 N. Boden, P. H. Jackson, K. McMullen and M. C. Holmes, Chem. Phys. Lett., 65 (1979) 476.
31 C. Rosenblatt, S. Kumar and J. D. Litster, Phys. Rev., A29 (1984) 1010; B. D. Larson and J. D. Litster, private communication.
32 P. G. deGennes, The Physics of Liquid Crystals, Clarendon, Oxford, 1974.
33 P. H. Keyes, Phys. Lett., A67 (1978) 132.
34 T. C. Lubensky, J. Chim. Phys. (Paris), 80 (1983) 31.
35 J. Thoen, H. Marynissen and W. Van Dael, Phys. Rev. Lett., 52 (1984) 204.